*Materials Science-Poland*, *Vol. 28*, *No. 2*, *2010*

# Synthesis, characterization and properties of nanocrystalline perovskite cathode materials

S. GHOSH, S. DASGUPTA*

Ceramic Membrane Division, Central Glass and Ceramic Research Institute,
Council of Scientific and Industrial Research, Kolkata 700 032, India

A simple low temperature synthesis route has been presented of preparing nanosized, single phased $LaFeO_3$, $La_{(1-x)}Sr_xFeO_3$ ($x$ = 0.3, 0.5) and $La_{(1-x)}Sr_xCo_{0.2}Fe_{0.8}O_3$ ($x$ = 0.2, 0.4) for cathode applications in ITSOFC. A soft chemical method has been applied, using tartaric acid as a template material and nitric acid as an oxidizing agent. Phase pure materials were obtained at temperatures ranging from 550 °C to 700 °C. The synthesized powders were characterized by TGA, XRD, SEM and FTIR analysis. The crystallite size was 45–50 nm, with the surface area of 14–20 $m^2/g$. Electronic conductivity of the material was found to increase upon increasing Sr concentration and the sintering temperature. High electronic conductivities of 355 S/cm and 545 S/cm were obtained at 400 °C for $La_{0.5}Sr_{0.5}Fe_2O_3$ and $La_{0.6}Sr_{0.4}Co_{0.2}Fe_2O_3$, respectively. Activation energy decreases with the increase in Sr concentration. The values of thermal expansion coefficients (TEC) of the materials are compatible with the TEC of the ceria-gadolinium oxide CGO interlayer between cathode layer and electrolyte.

Keywords: *electronic materials; chemical synthesis; X-ray diffraction; electrical conductivity*

## 1. Introduction

Solid oxide fuel cells (SOFCs) are environmentally friendly potential energy sources for the future production of electrical power, due to their high efficiency, low emission, multifuel activity and modularity. The most widely used fuel cell consists of a cathode, typically an $ABO_3$ ($LaMnO_3$) perovskite, an electrolyte (yttria-stabilized zirconia, YSZ) and an anode (Ni-YSZ cermet). The problem with this system is that it operates at high temperatures. Reduction of operating temperature to 550–700 °C is now the primary hurdle for the commercialization of SOFC. However a decrease in the operating temperature will decrease the cell performances of the conventional fuel cell, due to cathode overpotential. Hence, for ITSOFC applications, one seeks perovskites having high conductivity at low temperature.

*Corresponding author, e-mail: sdasgupta@cgcri.res.in

Lanthanum–strontium–cobalt ferrite (LSCF) is the best known mixed ionic electronic conductor used in intermediate temperature SOFC (ITSOFC) applications [1–3] and oxygen permeating membranes [4, 5]. A high electronic and ionic conductivity of LSCF over lanthanum–strontium manganite (LSM), makes it an attractive cathode material. The properties of their defect states have been examined extensively [6, 7]. The lower operating temperature of LSCF makes it possible to use cheaper interconnect materials and a wide range of sealing materials [8], thereby improving the reliability and long term stability of the fuel cell. However, it is reported that the insulating $SrZrO_3$ or the $LaZr_2O_7$ phase between LSCF and the YSZ electrolyte is formed during the sintering of the fuel cell. Therefore, buffers of ceria–gadolinium oxide (CGO), GDC or SDC were used as interlayers between the LSCF and the YSZ, in order to prevent Sr and La percolation [9].

Various methods of preparation of lanthanum ferrite (LF), lanthanum strontium ferrite (LSF) and lanthanum strontium cobalt ferrite (LSCF) have been reported. Preparation conditions are mainly responsible for morphological differences and the disparity in their electrochemical properties. Various synthesis routes comprise such methods as spray pyrolysis [10], coprecipitation method [11], citrate gelling method [12], modified citrate pyrolysis method [13], citrate method under effect of various pH [14], oxalate precipitation method [15] glycine nitrate technique [16, 17], sol gel route [18], mechanochemical method [19] and solution combustion using tetraformyltrisazine and oxalyl dihydride [20].

The present work describes the synthesis of $LaFeO_3$, $La_{(1-x)}Sr_xFeO_3$, ($x$ = 0.3, 0.5) $La_{(1-x)}Sr_xCo_{0.2}Fe_{0.8}O_3$, ($x$ = 0.2, 0.4) perovskite cathode materials by the tartarate template method, where phase pure perovskites were formed at temperature as low as 550–700 °C. Particle size, surface area studies, microstructure characterization, sintering behaviour, electrical properties and thermal expansion tests were carried out with the synthesized powder.

## 2. Experimental

*Syntheses.* Stoichiometric amounts of $La(NO_3)_3 \cdot 6H_20$ and $Fe(NO_3)_3 \cdot 9H_2O$ dissolved in 2M nitric acid were placed in a beaker. Tartaric acid in 1:2 molar ratio with respect to metal nitrates was added to the mixture. The mixture was heated under constant stirring on a hot plate until all the liquid had evaporated. The resultant mass was calcined at temperatures from 550 °C to 700 °C to obtain phase pure perovskite materials. The yield was 94%. The syntheses of $La_{(1-x)}Sr_xFeO_3$ and $La_{(1-x)}Sr_xCo_{0.2}Fe_{0.8}O_3$, ($x$ ranging from 0.2 to 0.5) was carried out by the same procedure, using nitrates of respective metals and tartaric acid as the chelating agent. All the chemicals were of analytical grade. Deionized water was used throughout the synthesis.

*Characterization of the materials*. Thermogravimetric studies of the uncalcined powders were carried out using a TG analyser (Model: Shimadzu TGA 50) in air, un-

der the heating rate of 20 °C/min in an alumina crucible. The temperature range was between room temperature and 800 °C.

X-ray diffractometry studies were carried out with an X-ray diffractometer (Philips, PW 1710) using a monochromatic $CuK_\alpha$ radiation from 10° to 70° ($2\theta$), in order to identify the phase and the crystal system. Crystallite size was determined based on Scherer's formula from the line broadening of the peak at around 32°. FTIR spectra were obtained using a Nicolet Model 5PC FTIR. A Sorpty 1750 surface area analyzer, based on the BET principle, was used to measure the specific surface area. The morphologies of the calcined powders and the microstructure of the fracture surfaces of the sintered samples were studied with a scanning electron microscope (model No. Leo: 430i).

The phase pure powders were ground and mixed with 1 wt. % of binder (poly (vinyl) butaryl acetate) compacted at 2 t pressure in a motor driven uniaxial hydraulic press, using a mould 10 mm in diameter. Green pellets thus obtained were sintered at 1100 °C and 1200 °C for 6 h. The densities of the sintered pellets were determined geometrically, as well as by immersion in kerosene and applying Archimedes principle.

The electronic conductivities of the sintered samples were measured in air by the four probe method at various temperatures. The samples for measurement of electronic conductivity were of rectangular shapes having dimensions 20 mm × 8 mm × 1.8 mm, fabricated exactly the same way as for sintering studies. Electroding was done with platinum wire, adhered to the surface by a coating of platinum paste, cured at 900 °C for 30 min. Electronic conductivity measurements were carried out in air at temperatures ranging from room temperature to 700 °C, or up to the saturation limit of the sample in a temperature controlled furnace.

Relative thermal expansion was measured in air, from room temperature to 800 °C, on samples of dimensions 25 mm × 8mm × 5mm sintered at 1200 °C. A dilatometer Netzsch Dil 402C model was used with $Al_2O_3$ as reference at the heating rate of 5 °C/min.

## 3. Results and discussion

### 3.1. Thermal analysis and FTIR studies

Figure 1 shows the comparative TGA plots of the prepared uncalcined precursors, i.e., $LaFeO_3$, $La_{(1-x)}Sr_xFeO_3$ and $La_{(1-x)}Sr_xCo_{0.2}Fe_{0.8}O_3$, by the tartarate route. Considerable weight loss was observed up to 400 °C followed by a slight weight loss in the 400–600 °C range. A negligible weight loss occurred between 600–650 °C.

The TG curves can be interpreted well based on FTIR studies (Fig. 2). A broad peak around 3440 $cm^{-1}$ in the green sample is due to the stretching mode of the hydroxyl group of bound water molecules, which gradually diminishes as the calcination temperature is raised to 700 °C. The peak at 2337 $cm^{-1}$ is due to ambient $CO_2$. The

broad peaks at around 1630 $cm^{-1}$ and at 1385 $cm^{-1}$ are due to carboxylate and nitrate groups, respectively.

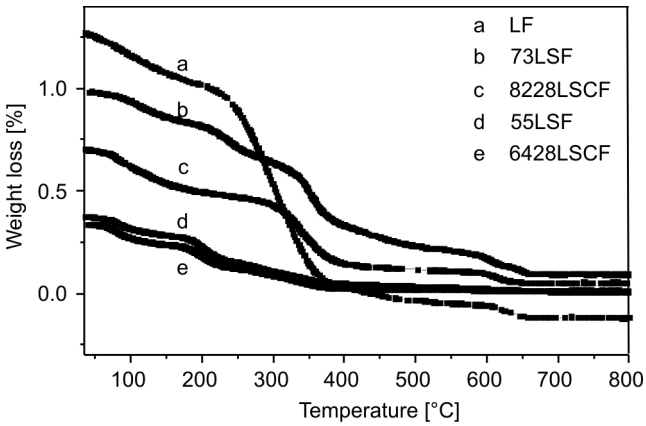


Fig. 1. TGA curves of $LaFeO_3$, $La_{(1-x)}Sr_xFeO_3$, and $La_{(1-x)}Sr_xCo_{0.2}Fe_{0.8}O_3$ precursors

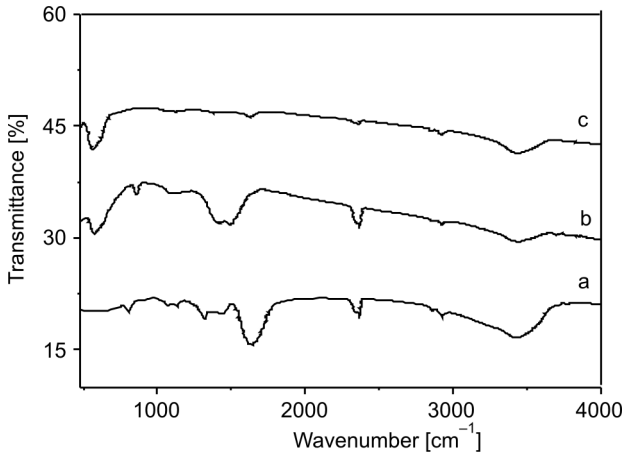


Fig. 2. FTIR spectra of $LaFeO_3$ uncalcined (a) and calcined at 550 °C (b) and 700 °C (c)

The carboxylate peak vanishes at 550 °C, whereas a broad band appears between 1400 $cm^{-1}$ and 1500 $cm^{-1}$ due to the bending vibration mode of bound water molecules and the $\upsilon_3$ mode of $CO_3^{2-}$ ions which disappears when calcination occurs at 700 °C. The peaks at around 1070 $cm^{-1}$ and 860 $cm^{-1}$ are attributed to the $\upsilon_1$ and $\upsilon_2$ modes of $CO_3^{2-}$ ions, respectively. When the sample is calcined at 700 °C, all these peaks disappear, leaving phase pure perovskite, which is highly consistent with our TGA and XRD data.

### 3.2. X-ray analysis

Figure 3 shows the X-ray diffraction patterns of $LaFeO_3$, calcined at various temperatures. The XRD pattern reveals that phase pure material is formed at ca. 550 °C. Results of the TG and IR analyses show that there are, still some impurity phases, which are not detectable by XRD.

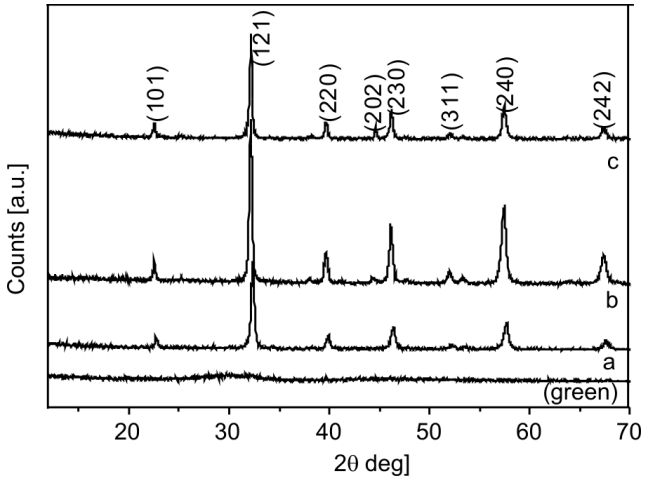


Fig. 3. XRD patterns of $LaFeO_3$ calcined at 550 °C (a), 600 °C (b) and 700 °C (c)

Since IR spectroscopy is a much more sensitive tool, it can only support the complete formation of phase pure material. Phase formation begins at 550 °C, and complete phase pure perovskite material was obtained on calcining the powder at 700 °C for 3 h. The line broadening decreased as the calcination temperature increased, as seen in the figure for the (121) plane of pure $LaFeO_3$. The primary particles were of nanosize dimensions, agglomerating during calcination. The average crystallite size calculated using Scherrer's formula was found to be ca. 45–50 nm.

Figure 4 shows the X-ray diffraction pattern of $La_{0.7}Sr_{0.3}FeO_3$ (73LSF) and $La_{0.8}Sr_{0.2}Co_{0.2}Fe_{0.8}O_3$ (8228LSCF) calcined at 700 °C. Traces of $Co_3O_4$ were found in $La_{0.8}Sr_{0.2}Co_{0.2}Fe_{0.8}O_3$, but they disappeared completely when calcining the sample at 800 °C [21].

The uniqueness of tartaric acid as a chelating agent in the synthesis of $BiFeO_3$ has been reported earlier. The formation of heteroatomic polynuclear complexes brings the metal atoms in close proximity with each other, which decays in the presence of nitric acid to give the product [22]. Our earlier work with oxalic acid [23] as a chelating agent in synthesizing $BiFeO_3$ reports the formation of transition metal ferrioxalate $Bi[Fe(ox)_3]$ intermediate which undergoes *in situ* decomposition by $HNO_3$, resulting in the formation of the product. The role of tartaric acid as a chelating agent in synthesis of $LaFeO_3$ probably consists in the formation of transition metal tartrato lanthanate(III) [24] precursor ($M[La(C_4H_4O_6)_3]\cdot xH_2O$).

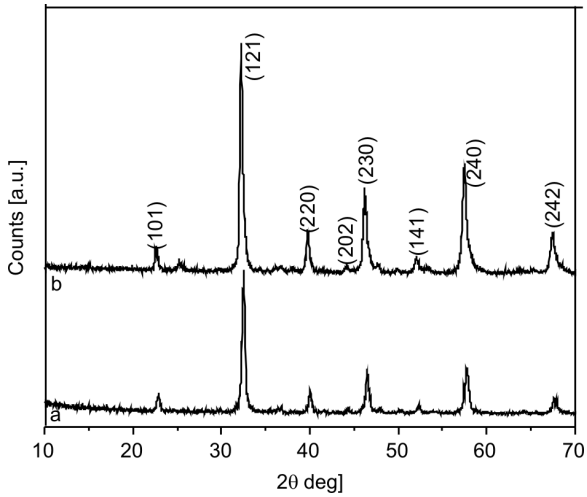


Fig. 4. XRD pattern of: a) $La_{0.7}Sr_{0.3}FeO_{3-x}$, b)$La_{0.8}Sr_{0.2}Co_{0.2}Fe_{0.8}O_3$ calcined at 700 °C

In this case $Fe[La(C_4H_4O_6)_3]\cdot 10H_2O$, like $La[La(C_4H_4O_6)_3]\cdot 10H_2O$ may be formed, as was observed by Deb [25] in the synthesis and thermolysis of lanthanum(III) tris tartrato lanthanate (III) decahydrate precursors. Here also, iron (III) tris tartrato lanthanate(III) decahydrate, $Fe[La(C_4H_4O_6)_3]\cdot 10H_2O$ formed by reaction with tartarate ligand, undergoes *in situ* decomposition, which occurs towards the end of the reaction, when the $HNO_3$ concentration is high enough to oxidize the precursor, resulting in the generation of $NO_2$, $CO_2$ and water vapour, along with the product.

### 3.3. Surface area analysis

The surface area of the phase pure powders was determined using the BET principle. The measured surface area of the synthesized powders was in the 14–20 $m^2/g$ range (Table 1). $La_{0.5}Sr_{0.5}Fe_2O_3$ (55LSF) exhibits a maximum surface area of 19.10 $m^2/g$, which is much higher than the surface area of powder synthesized by the citrate method [26].

Table 1. Surface areas of various powders

| Compound | Surface area [$m^2/g$] |
|---|---|
| 73LSF | 14.00 |
| 55LSF | 19.10 |
| 8228LSCF | 13.58 |
| 6428 LSCF | 15.22 |

### 3.4. Morphology and microstructure analysis

Figure 5a shows the microstructure of $LaFeO_3$ powders calcined at 700 °C for 3 hs. The crystallite sizes are in good agreement with that obtained from XRD. Spherically shaped particles are seen to exhibit considerable agglomeration.

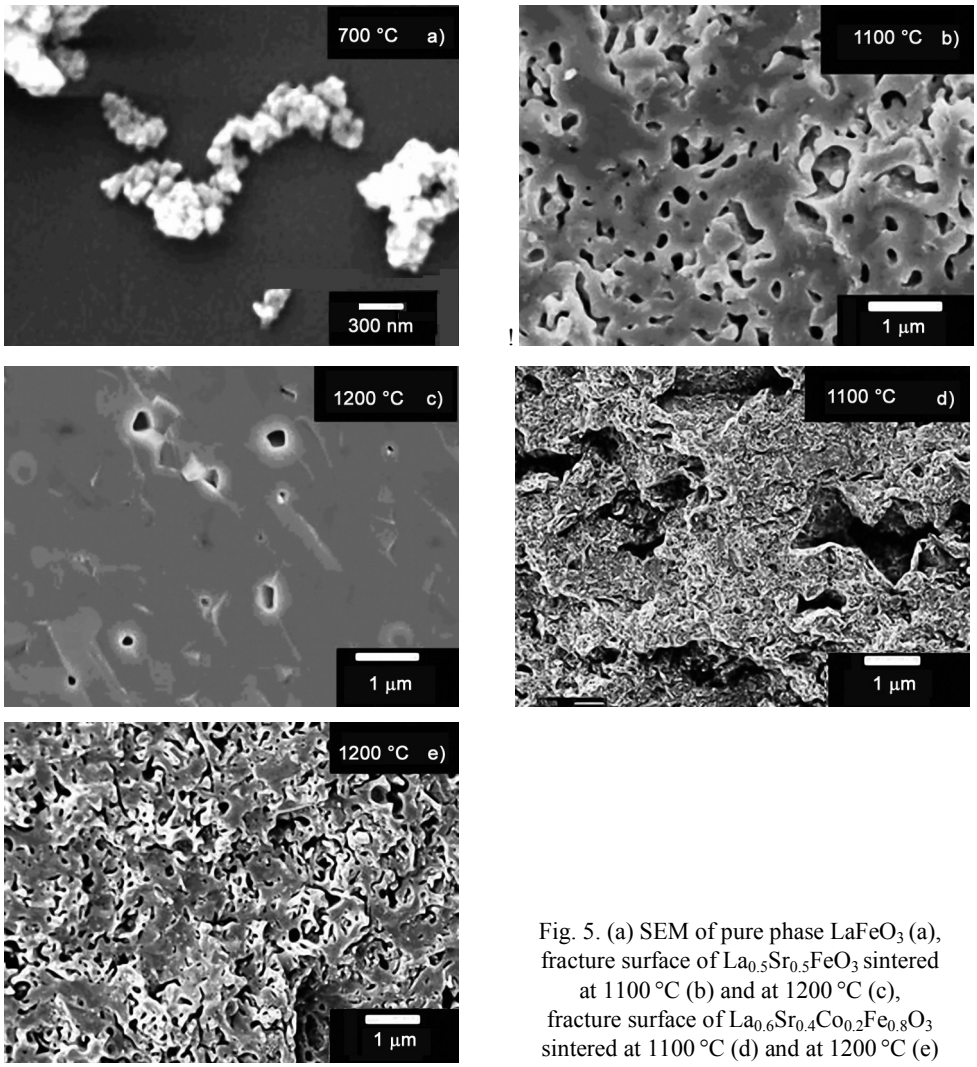


Fig. 5. (a) SEM of pure phase $LaFeO_3$ (a), fracture surface of $La_{0.5}Sr_{0.5}FeO_3$ sintered at 1100 °C (b) and at 1200 °C (c), fracture surface of $La_{0.6}Sr_{0.4}Co_{0.2}Fe_{0.8}O_3$ sintered at 1100 °C (d) and at 1200 °C (e)

Figures 5b–e show the microstructure of the fracture surface of $La_{0.5}Sr_{0.5}Fe_2O_3$ (55LSF) and $La_{0.6}Sr_{0.4}Co_{0.2}Fe_2O_3$ (6428LSCF) sintered at 1100 °C and 1200 °C. Porous and inhomogeneous structures are seen in samples sintered at 1100 °C, whereas a highly dense structure is seen in samples sintered at 1200 °C. Adjusting the sintering temperature improves the microstructure and thereby improves the electronic conductivity.

### 3.5. Conductivity studies

Electronic conductivities were measured by the four probe DC principle [27]. Figures 6 and 7 show the dependences of the logarithm of electrical conductivity on the reciprocal of temperature ($\lg\sigma(1/T)$) for the synthesized powders sintered at 1100 °C and 1200 °C.

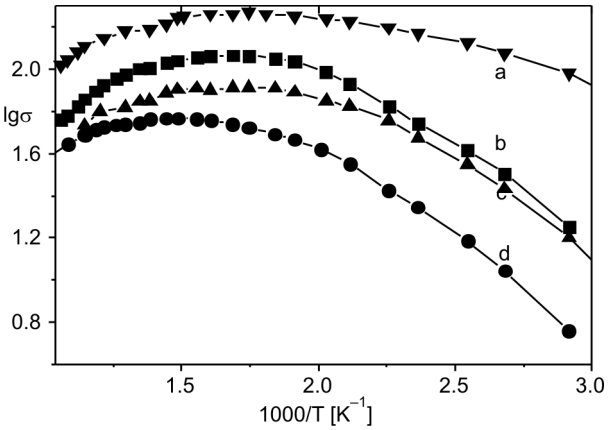


Fig. 6. Dependences of $\lg\sigma$ on the reciprocal temperature of:
a) $La_{0.6}Sr_{0.4}Co_{0.2}Fe_{0.8}O_3$ (6428LSCF), b) $La_{0.5}Sr_{0.}5Fe_2O_3$ (55LSF),
c) $La_{0.8}Sr_{0.2}Co_{0.2}Fe_{0.8}O_3$ (8228LSCF), d) $La_{0.7}Sr_{0.3}FeO_3$ (73LSF)
sintered at 1100 °C in air

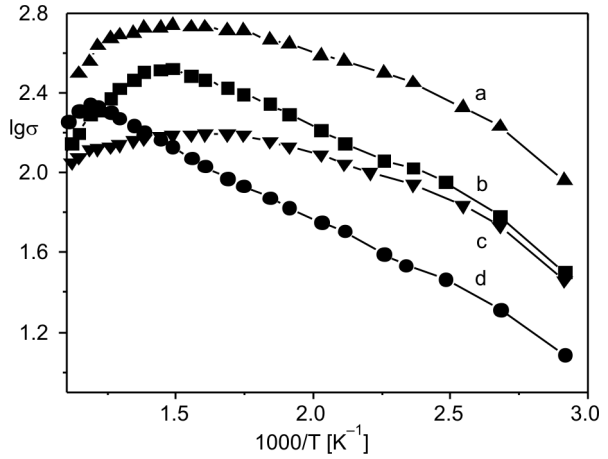


Fig. 7. Dependences of $\lg\sigma$ on the reciprocal temperature of:
a) $La_{0.6}Sr_{0.4}Co_{0.2}Fe_{0.8}O_3$ (6428LSCF), b) $La_{0.5}Sr_{0.}5Fe_2O_3$ (55LSF),
c) $La_{0.7}Sr_{0.3}FeO_3$ (73LSF), d) $La_{0.8}Sr_{0.2}Co_{0.2}Fe_{0.8}O_3$ (8228LSCF) sintered at 1200 °C in air

As expected, the figures show that the conductivity is highly dependent on the sintering temperature, i.e, the conductivity increases with the increase in the sintering

temperature. The conductivity of most of the powders is found to increase with temperature, up to 400 °C and in some cases up to 500 °C. A steep decline in conductivity is observed for the samples treated above these temperatures, suggesting that a semiconductor-to-insulator transition occurs. In all cases, the conductivity increased 2- or 3-fold with the increase in the sintering temperature, e.g. the conductivities at 500 °C of 8228LSCF sintered at 1100 °C and at 1200 °C are 65.74 S/cm and 187.08 S/cm, respectively. Increasing the sintering temperature significantly improves the conductivity, which is due to the better densification at higher temperatures. 55LSF shows a maximum conductivity at 420 °C of 355 S/cm and 263 S/cm at 500 °C. Bongio et al. [28] reported a maximum conductivity of 352 S/cm at 550 °C for the same composition. The authors have therefore achieved comparable conductivity at a much lower temperature, which may be due to reduced crystallite sizes and better sinterability.

### 3.6. Activation energy

The activation energies of the sintered samples were calculated from the slopes of $\log(\sigma T)$ vs. $T^{-1}$ plots, according to the Arrhenius equation:

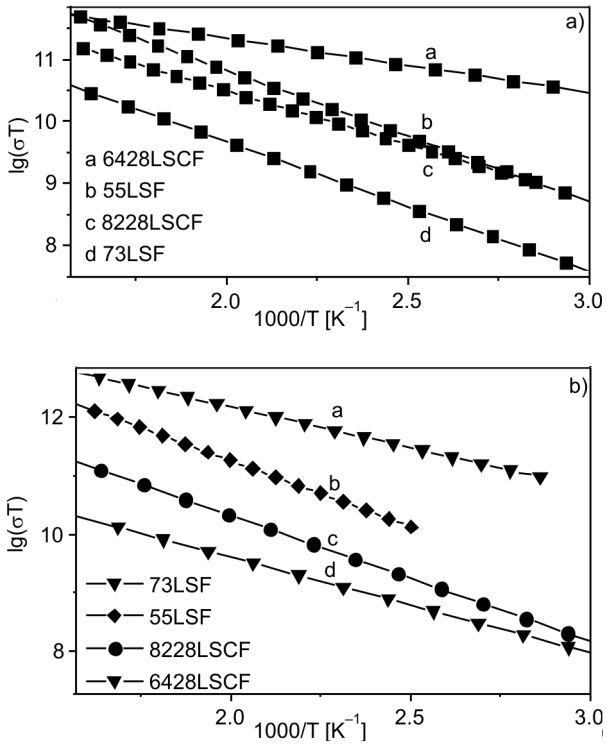


Fig. 8. Activation energy for samples sintered at 1100 °C (a) and at 1200 °C (b)

$$\sigma = \frac{A}{kT}\exp\left(-\frac{E_a}{kT}\right)$$

where $A$ is a constant, $E_a$ is the activation energy, $k$ is the Boltzmann constant, $T$ is the absolute temperature.

Figures 8a, b show the linear plots of $\log(\sigma T)$ vs $1000/T$ for the temperature ranges where the conductivity increased with temperature for the samples sintered at 1100 °C and 1200 °C, respectively [29]. The activation energies range from 0.025 eV to 0.194 eV in $La_{(1-x)}Sr_xFeO_3$, which is in close agreement with the value reported by Omata et al. [30]. As expected, the activation energy becomes lower if the strontium content is increased. In the case of $La_{(1-x)}Sr_xCo_{0.2}Fe_{0.8}O_3$, the $E_a$ value ranges between 0.075 eV and 0.185 eV, which is in close agreement with the data reported by Tai et al. [31].

### 3.7. Measurement of the thermal expansion coefficients (TEC)

The cathode material should have matched TEC and sufficient stability with the electrolyte to avoid thermal mismatching and percolation. Figure 9 shows the TEC graphs of the materials (sintered at 1200 °C) for temperatures ranging between room temperature and 800 °C.

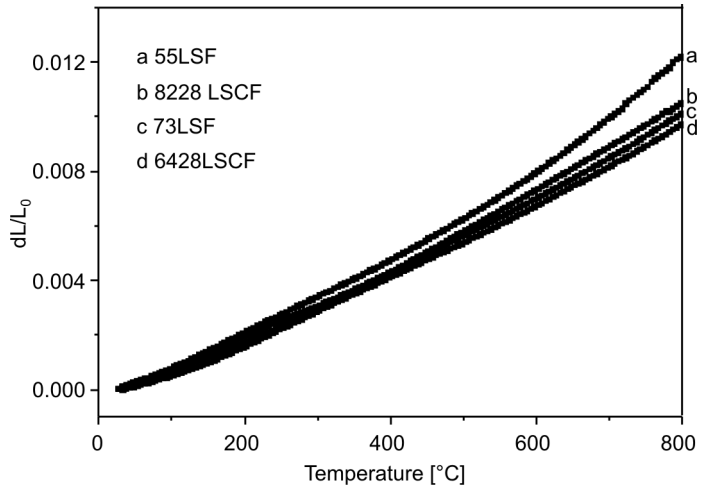


Fig. 9. Temperature dependences of the thermal expansion coefficients of Sr and Co doped samples

The TEC of the synthesized powders does not match with conventional 8% YSZ electrolyte ($\alpha_{YSZ}$ = 10.8×510$^{-6}$ K$^{-1}$ for 30–1000 °C) which is normally used in the SOFC. The TEC of 6428LSCF is found to be in well agreement with that for the CGO layer ($\alpha$ = 12.671×10$^{-6}$ K$^{-1}$). Therefore a buffer layer of CGO has to be applied between LSCF and YSZ for matching TEC which will also prevent the percolation of Sr

and La to the YSZ layer hindering the formation of $SrZrO_3$ and $La_2Zr_2O_7$. 73LSF and 8228LSCF are also close matches for CGO interlayer as their TEC values are in accordance.

## 4. Conclusion

A low temperature method was used for the synthesis of nanosized lanthanum ferrite and doped lanthanum ferrite materials by simple solution evaporation technique. The synthesized materials were characterized and sintered at various temperatures, in order to study their suitability for ITSOFC applications. High conductivities of the synthesized materials at lower temperatures show that they are best suited as cathode materials for intermediate temperature SOFC applications. The activation energy can be reduced from 0.180 eV to 0.075 eV by appropriate increase of the strontium content. The TECs of the synthesized materials have a similar profile to the TEC of the CGO interlayer.

**Acknowledgement**

One of the authors (S. G.) is grateful to the CSIR for awarding SRF (No. 31/15(58)/06-EMR-I). Thanks are due to Dr R. N. Basu for providing the laboratory facilities. Thanks are also due to the Director CGCRI, for allowing us to publish this paper.

## References

[1] KIM W.H., SONG H.S., MOON J., LEE H.W., Solid State Ionics, 177 (2006), 35.
[2] QIANG F., NING S.K., ZHANG N.Q, ZHU X.D., SHI X.D., LE R., ZHOU D.R., J. Power Sources, 168 (2007), 338.
[3] QIU L., ICHIKAWA T., HIRANO A., IMANISHI N., TAKEDA Y., Solid State Ionics, 158 (2003), 55.
[4] LEE S., LEE K.S., WOO S.K., KIM J.W., ISHIHARA T., KIM D.K., Solid State Ionics, 158 (2003), 287.
[5] TERAOKAY., HONBE Y., ISHII J., FURUKAWA H., MORIGUCHI I., Solid State Ionics, 152 (2002), 681.
[6] MISUZAKI J., SASAMOTO T., CANNON W.R., BOWEN H.K., J. Am. Ceram. Soc., 66 (1983), 247.
[7] BUCHER E., SITTE W., Solid State Ionics, 173 (2004), 23.
[8] JIANG S.P., ZHNAG J.P., ZHENG X.G., J. Eur. Ceram. Soc., 22 (2002), 361.
[9] MAI A., HANNAPPEL V.A.C., UHLENBRUCK S., TIETZ F., STOVER D., Solid State Ionics, 176 (2005), 1341.
[10] HOLTAPPELS P., VOGT U., SCHINDLER H., GUT B., 5th European Solid Oxide Fuel Cell Forum, J. Huijismans (Ed.), Lucerne, Switzeland (2002), pp. 103–107.
[11] ZENG Y., LIN Y.S., SWARTZ S.L., J. Membrane Sci., 150 (1998), 87.
[12] DUOY A., Int. J. Inorg. Mater., 3 (2001), 699.
[13] SFEIR J., VAUCHER S., HOLTAPPELS P., VOGT U., SCHINDLER H.J., HERLE J.V., SUVOROVA E., BUFFAT P., PERRET D., XANTHOPOLOUS N., BUCHELI O., J. Eur. Ceram. Soc., 25 (2005), 1991.
[14] LI S., XU N., J. Mater. Sci. Lett., 21 (2002), 245.
[15] WU Z., ZHOU W., JIN W., XU N., Materials, Interf. Elctrochem. Phen., 52 (2005), 769.
[16] RALPH J.M., ROSSIGNOL C., KUMAR R., J. Electrochem. Soc., 150 (2003), 1518.
[17] LEI Z., ZHU Q., ZHAO L., J. Power Sources, 161 (2006), 1169.
[18] GE L., ZHOU W., RAN R., SHAO Z., LIU S., J. Alloys Comp., 450 (2008), 338.

[19] YAKOVLEVA I.S., ISUPOVA L.A., TSYBULYA S.V., CHERNYSH A.V., BOLDYREVA N.N., ALIKINA G.M., SADIKOV V.A., J. Mater. Sci., 39 (2004), 5517.
[20] SURESH K., PANCHAPAGESAN T.S., PATIL K.C., Solid State Ionics,, 126 (1999), 299.
[21] TIETZ F., RAJ I.A., ZAHID M., STOVER D., Solid State Ionics, 177 (2006), 1753.
[22] GHOSH S., DASGUPTA S., SEN A., MAITI H.S., J. Am. Ceram. Soc., 88 (2005), 1349.
[23] GHOSH S., DASGUPTA S., SEN A., MAITI H.S., Mater. Res. Bull., 40 (2005), 2073.
[24] DEB N., J. Anal. App. Pyrolysis, online availability 27.03.2008.
[25] DEB N., J. Thermal An. Calorim., 78 (2004), 227.
[26] MURATA K., FUKUI T, ABE H., NAITO M., NOGI K., J. Power Sources, 145 (2005), 257.
[27] RIETVELD G., KOIJMANS C.V., HENDERSON L.C.A., HALL M.J., HARMON S., WARNECKE P., SCHUMACHER B., IEEE Trans. Inst. Meas., 52 (2003), 449.
[28] BONGIO E.V., BLACK H., RASZEWSKI F.C., EDWARDS D., MCCONVILLE C.J., AMARAKOON V.R.W., J. Electroceram., 14 (2005), 193.
[29] KOSTOGLOUDIS G.C., FTIKOS C., Solid State Ionics, 126 (1999), 143.
[30] OMATA T., IKAWA H., FIJITSU S., UEDA N., HOSONA H., KAWAZOE H., Solid State Com., 97 (1996), 411.
[31] TAI L.W., NASRSLLAH M.M., ANDERSON H.U., SPARLIN D.M., SEHLIN S.R., Solid State Ionics, 76 (1995), 259.

*Received 2 December 2008*
*Revised 9 February 2009*